Scientific Research Publishing

Materials Sciences and Applications, 2025, 16(6), 327-347
https://www.scirp.org/journal/msa
ISSN Online: 2153-1188
ISSN Print: 2153-117X

Prediction of Physic-Mechanical Properties of Geopolymers Based on Recycled Thermoplastic Materials for Stabilizing Buildings: Case of Mara and Toukra Sites of N'Djamena

Innocent Allahdoumbaye[1,2], Pagore Frédéric Djoda[2,3*], Pagna Bertin Kagonbé[4], Gomdje Valery Hambaté[5], Raïdandi Danwé[2]

[1]Department of Civil Engineering, Faculty of Engineering Sciences and Technology, Polytechnic University of Mongo, Mongo, Chad
[2]Department of Civil Engineering and Architecture, National Advanced School of Engineering, University of Maroua, Maroua, Cameroon
[3]Laboratory of Mechanic and Material Processing (LMP), UFD SI, University of Douala, Douala, Cameroun
[4]Local Materials Authority Promotion (MIPROMALO), Yaoundé, Cameroon
[5]Department of Textile and Leather Engineering, National Advanced School of Engineering, University of Maroua, Maroua, Cameroon
Email: *frederic.djodap@univ-maroua.cm, djodap@yahoo.fr

How to cite this paper: Allahdoumbaye, I., Djoda, P.F., Kagonbé, P.B., Hambaté, G.V. and Danwé, R. (2025) Prediction of Physic-Mechanical Properties of Geopolymers Based on Recycled Thermoplastic Materials for Stabilizing Buildings: Case of Mara and Toukra Sites of N'Djamena. *Materials Sciences and Applications*, **16**, 327-347.
https://doi.org/10.4236/msa.2025.166019

Received: May 9, 2025
Accepted: June 8, 2025
Published: June 11, 2025

Abstract

Early settlement collapses led us to stabilize earth bricks in the Mara region and make predictions in Toukra. This work demonstrates the improvement in the mechanical properties of earth bricks combined with recycled polypropylene and polyethylene thermoplastics. This is due to the compatibility between the clay layers and the molecular chains derived from these polymers. Indeed, the investigations carried out on the materials of the two Mara sites first focused on geochemistry, which showed the presence of silica oxides SiO_2 (59.11% - 63.28%), aluminum Al_2O_3 (12.62% - 12.78%) and iron Fe_2O_3 (6.12% - 6.97%) as major elements. Alkaline and alkaline earth elements such as potassium K_2O (3.06% - 3.15%), titanium TiO_2 (0.98% - 1.15%), sodium Na_2O (1.02% - 1.13%), calcium CaO (1.01% - 2.13%), magnesium MgO (0.58% - 1.13%) then appear in small quantities. These oxides come from quartz, kaolinite, feldspar, illite and many other constituents of the ore confirmed by DRX, ATR FTIR and ATG/DTA. The vibrational movements observed with the presence of polypropylenes and polyethylene's favored the physicochemical interactions with the mineral oxides. The rheological character of this polymer matrix made it possible to plug the micropores of the clay sheets by acting in a compatible manner with the oxides present. All these samples lose

very little mass, 21.12% on average according to the TGA. They have an energy conservation capacity and degrade around 498˚C. All of these microstructural analyses allowed us to predict good water absorption behavior and good mechanical performance. Some formulations provided less than 2% water absorption in 10 days of immersion. Compressive strength ranges from 12.28 to 17.35 MPa at Mara and from 10.22 to 14.22 MPa at the Toukra site. This could be generalized to other areas sharing the risk of early collapse.

Keywords

Stabilization, Earth Bricks, Thermoplastic, Microstructure, Physic-Mechanical Behavior

1. Introduction

The use of resources from our earth's crust in the various areas of housing construction is very popular in developing countries. Populations are almost condemned to use them because of their precariousness and their availability around our ecosystem [1]. Earths-materials have varied behaviors because they have multifaceted layers. Having no way to verify them, let alone predict their behavior in operation, these populations suffer dramatic consequences. Indeed, they build with materials from their settlement area. They find themselves confronted with bad weather linked to climate change and floods which are the main causes of the early collapse of said constructions. This makes these populations unstable and vulnerable. This problem of early collapse of buildings in the outlying districts of the city of N'Djamena challenges the public authorities as well as researchers. One of the objectives we are pursuing is the stabilization of earth bricks from each locality by incorporating recycled thermoplastics. However, investigations on similar materials will be carried out to understand their behavior. First, the evaluation of oxides with their more or less clayey character [2] is necessary to give an orientation on these soils in some properties [3]. This is how work is carried out on the microstructural level to have perfect control of said soils [4]. The determination of the constituents of the soils is for the most part requested based on geochemical, geotechnical and even mineralogical studies [5] in order to enhance their value in construction work [6]-[8]. The research carried out on the essence of these oxides will allow us to have an idea on the intrinsic characteristics of said constituents. This will have an impact on the formation of chemical-mechanical bonds that these minerals could generate with other constituents like biopolymers [9] to establish high-performance composites. This is why predominantly sandy areas can have elastoplastic properties with porosity influencing their ability to retain torrential rains. Nowadays, polymers of various origins are used to strengthen the capacity to manage the interfacial and interphase properties of mineral-type oxides. Having noted that the soils of N'Djamena in general are predominantly siliceous [10] [11], the use of thermoplastic polymers as a contribution could further

stabilize the soaked earth bricks. It should be noted that the presence of alumina/silica oligomers generates a crystallizable amorphous network [12] [13]. It is therefore indicated to form a system that identifies with a geopolymerization that would allow this polymer network to crosslink in order to form a denser network [14] [15]. The types of ores will be identified by X-ray diffraction analyses to confirm the results of geochemistry [16]. The cohabitation of polymers with ores gives rise to vibrational movements that must be confirmed by FTIR analyses [17] [18] Mechanisms related to phase change such as evaporation, dehydration and then crystallization [19] influence the microstructure. A substantial thermal analysis is essential to evaluate the implementation conditions in order to predict the physical and mechanical properties of said materials [20]-[23]. Specifically, it will be a question of evaluating their capacity to preserve their essential constituents with the evolution of temperature. Thermogravimetric analysis will be requested to determine the loss of mass as a function of temperature [24]. This will be coupled with differential thermal analysis to determine the different transformation phases of the designed materials [25]. These microstructural analyses will be carried out to make a prediction of the physical and mechanical properties from the formulations made in order to determine a perfect mixture of constituents to inform the target populations.

2. Materials and Methods

2.1. Sampling Methods and Geographical Coordinates

The materials used were collected from the Mara and Toukra localities. These earth materials will be combined with selected recycled plastics, primarily using polypropylenes and polyethylene's. These two components produced the samples shown in **Figure 1**.

Figure 1. Samples from the Mara and Toukra sites.

2.2. Geochemistry Study by X-Ray Fluorescence Spectroscopy (XRF)

X-ray fluorescence spectroscopy (XRF) method was employed to determine the chemical composition of the Mara and Toukra side. The experiment was performed using a Philips XRFSPW 1404 spectrometer at the Cameroon cement plant (Cimencam) of Figuil in Cameroon (Lafarge group).

2.3. Structural Analysis by X-Ray Diffraction (XRD)

In order to determine the structural information of the sample, powders studied in the Mara and Toukra sites, an analysis is carried out using a Bruker diffractometer whose characteristics are: Cu Kα1 anticathode with wavelength variation at λ = 1.5418 Å, voltage V = 40 kV and intensity I = 30 mA. The angle is used on 6˚ < 2θ < 80˚ with steps of 0.02˚ and a time-frequency in steps of 2 s, in the Bragg-Brentano θ/θ configuration. The maximum intensities of the models used are both qualitative and semi-quantitative [25] [26].

2.4. Attenuated Total Reflectance Fourier Transform Infrared Radiation Analysis (ATR-FTIR)

The chemicals bonds and clay materials surface functional groups were determined by ATR-FTIR. The FTIR spectra were collected using a Perkin Elmer Frontier spectrometer equipped. Data were collected under ambient conditions from 400 - 4000 cm^{-1} using 16 scans with a resolution of 1 cm^{-1}. All spectra were background subtracted, baseline-corrected, and normalized using the strongest peak at 1101 cm^{-1}. All samples were ground to a fine powder of ≤10 μm particle size. Background spectra were collected under ambient conditions with the blank zinc selenide crystal.

2.5. Thermogravimetric Analysis (TGA) and Differential Thermal Analysis (DTA)

TGA and DTA experiment was investigated to bring out the transition signals correlated to mass losses and/or phase changes. The analysis was performed on a SetaramLABevo TG-DSC 1600˚C dispositive, running under Argon flow. Starting from the room temperature, samples were heated up to 1200˚C within a ramp of 10 to 40˚C·min^{-1}. The DTA survey was run in an air flow, with Al_2O_3 crucibles.

2.6. Water Absorption and Compressive Strength Tests

2.6.1. Water Absorption Test

This test was conducted in the chemical engineering laboratory of the National School of Public Works in N'Djamena. An oven was used to dry the samples at a temperature of 105˚C to remove absorbed moisture. After cooling the samples in a desiccator, they were weighed (m_0) using a high-quality precision digital balance. The specimens were then immersed in a container of distilled water at room temperature. This procedure was repeated every 24 hours after sampling, carefully removing the surface water with absorbent paper, and the specimens were re-

weighed (m). This test continued until the mass (m) tended towards a constant. A series of four specimens was used per formulation. The mass percentage is given by the relationship:

$$W\% = \frac{m - m_0}{m_0} 100 \quad (1)$$

2.6.2. Compressive Strength Test

This test is used to assess compressive strength. The maximum breaking load is recorded during the test. Strengths are assessed at 7 days and then at 28 days of age using a hydraulic compression testing machine capable of applying loads up to 150 kN. The compression device accommodates specimens measuring 4 × 4 × 16 cm^3. The strength value considered is the average of the crushing stress of four specimens.

3. Results and Interpretations

3.1. Geochemical Characterization of Studied Soils

The XRF chemical analyzes give the quantities of the different major chemical elements of the clay materials studied (Table 1). Observation of these results shows overall that samples studied are mainly made up of SiO_2, Al_2O_3 and Fe_2O_3 and a small proportion of MgO, MnO, CaO, Na_2O, K_2O and P_2O_5.

Table 1. Geochemical composition of clay materials from the sites studied.

Oxides	SiO_2	Al_2O_3	Fe_2O_3	K_2O	MgO	TiO_2	P_2O_5	CaO	Na_2O	Mn_2O_3	*LOI*	SiO_2/Al_2O_3
Mara	63.28	12.62	6.12	3.06	0.58	1.15	0.04	1.01	1.13	0.09	10.92	5.62

Table 1 presents the results of geochemical analyses of the Mara sites. The data spontaneously display major elements such as oxides SiO_2 at 63.28% and Al_2O_3 at 12.62%; to which can be added Fe_2O_3 at 6.12%. The presence of alkali and alkaline earth metals is remarkable: potassium K_2O at 3.06%, titanium TiO_2 at 1.15%, sodium hydroxide Na_2O at 1.13%, calcium CaO at 1.01%, and magnesium MgO at 0.58%. Some constituents such as manganese Mn_2O_3 at 0.09% and phosphorus P_2O_5 at 0.04% appear negligible.

The loss on ignition at this site averages 10.92% and is relatively low. The main minerals are clearly shown in Table 1. This geochemical analysis shows the predominance of silica followed by alumina and iron at the two sites covered by this study. Loss on ignition is relatively low across the entire study area. Alkali and alkaline earth minerals are present despite their low value.

These samples have somewhat similar geochemical characteristics. Indeed, the variations in major element contents are relatively strong in both sites. The main oxides in order of importance are silica (SiO_2), alumina (Al_2O_3), iron (Fe_2O_3), alkali and alkaline earth (K_2O, CaO and MgO) and titanium (TiO_2). The silica (SiO_2) contents vary from 59.11% to 63.28% for all the samples analyzed. These main oxides are generally high compared to other sites in Ndjamena [10]. As a result,

these soils are of the clay type mainly composed of alumina silicate of quartz silica in predominance. These results agree with the work of Kagonbé [27], where the soils of the Sudano-Sahelian zones with contrasting seasons are mainly composed of silica.

The high amounts of alumina (Al_2O_3) predispose these soils to clay minerals such as kaolinite, highlighting a geochemical process called monosialization followed by bissialization. Another high element, Fe_2O_3, is thought to come from hematite, identified through the decomposition of clay minerals. The low carbonate mineral contents are observed by the low values of CaO and MgO in **Table 1**. The presence of potassium and sodium oxide suggests that the clay raw material is composed of illite.

The loss on ignition highlights the loss of moisture contained in these samples through the dehydroxylation reactions of clay minerals in general, followed by the decomposition of carbonates under the effect of temperature changes. The other fluxing elements could be confirmed by appropriate thermal analyses.

3.2. X-Ray Diffractogram Analysis

The diffractograms of the T20P and T35P samples from Mara are presented in **Figure 2**. They show that the addition of recycled thermoplastics in small quantities and at different proportions does not affect the crystallographic nature of these soil samples, on the one hand, and on the other hand, the amount of clay does not influence the nature of its intrinsic microorganic constituents. Therefore, the nature of the sharp peaks in these different samples reflects the crystalline nature of these materials.

These diffractograms show that these soils are composed of primary minerals such as quartz and feldspar; then secondary minerals such as kaolinite, smectite, and others that have appeared, such as montmorillonite and calcite such as hydroculumite. The presence of hydrated calcium chloroaluminates can be added to this diffractogram. Focal lengths ranging from 1.80 Å to 2.09 Å in this figure indicate the presence of calcium carbonate, calcite, and even alkali sulfates; this depends on the material's processing temperature. This confirms the presence of inter-reticular structures specific to the structural arrangement of calcite. This will have an impact on the mechanical properties of the clay in these samples.

Kaolinite is found in the reflection at 7.70 Å and 3.14 Å. Quartz, the majority mineral, is identified by reflections at 3.33 Å, 2.43 Å, 2.22 Å, 2.10 Å, 1.94 Å, 1.67 Å, 1.53 Å, 1.43 Å, 1.38 Å, 1.30 Å, 1.27 Å and 1.21 Å. Feldspar initially appears at 1.80 Å on all samples and then transforms into alkali sulfate under high temperature. Also, at 3.78 Å, we have plagioclase feldspar and also at 4.08 Å on this Mara site. The reflection peaks are fine-sized, which is characteristic of crystallites. These reflections for all these samples indicate that these constituents coexist. Smectite has a dioctahedral character; kaolinite around 7.70 Å is a mineral phase that easily associates with neighboring constituents such as smectite, quartz (3.33 Å) and potassium feldspars (4.08 Å). This good quantity of quartz with the con-

tribution of kaolinite is an asset for a good formulation and stabilization of compressed earth bricks.

The elongated shape of the characteristic peaks of these minerals indicates that they are crystallized [10]. The intensity of the quartz peaks displays their predominance throughout the mineralogical sphere. The variations observed in the mineralogy of these clayey soils may be linked to the climatic conditions of the entire region, in particular to the seasonal contrast due to the imbalance of the two seasons; namely a long dry season and a short rainy season [28] [29].

This explains their differential erodibility. This seasonal phenomenon, which leads to uncontrolled behavior of these soils, finds a favorable solution with the incorporation of polymer particles such as recycled polypropylene and polyethylene. The hydroxyl groups, carbonates, and multiple oxides from the minerals mentioned above are assets for combining efforts to consolidate strong bonds in order to obtain materials that meet the desired structural performance criteria.

Admittedly, the dual presence of smectite and kaolinite generates a crystallochemical process called bissialitization, which hardly ensures the desired consolidation of the existing constituents. The incorporation of thermoplastics can thus play an important role in their stabilization, which will improve the physical and mechanical properties of these materials.

It should be noted that the quantity of thermoplastics has no influence on the presence of the identified minerals in the formulated material. However, this quantity does influence the kinetics of crosslinking with the oxides present.

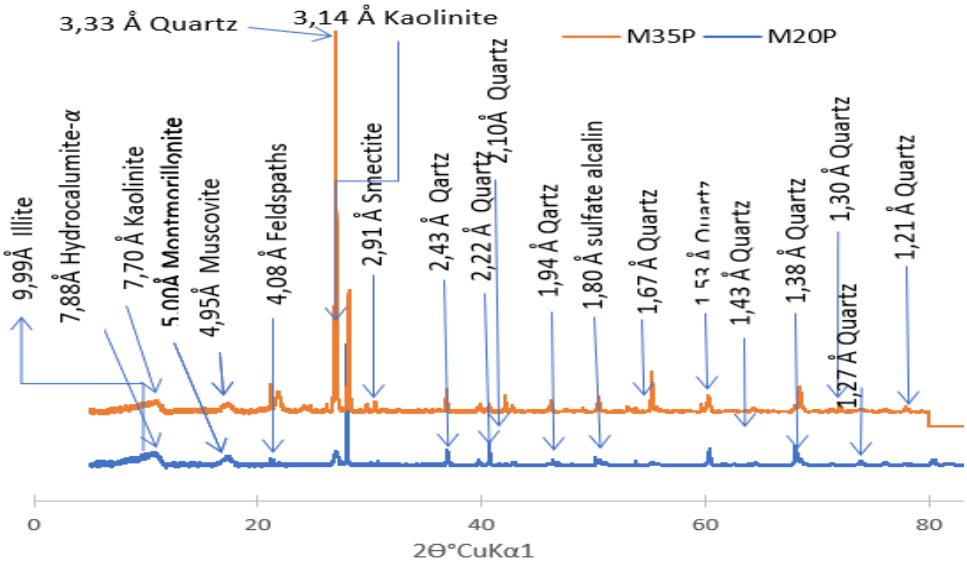

Figure 2. X-ray diffractograms of Mara samples.

3.3. ATR FTIR Analysis

The FTIR analyses of these samples involve interpretations of both thermoplastic polymers and clay minerals. This part of the study follows the XRD. The organic and mineral compounds are studied together to analyze their intermolecular co-

existence in order to interpret the compatibility of their structures. The chemical species present are analyzed through their different vibrational motions. The recording interval of our samples ranges from 4000 to 400 cm^{-1} and presents vibration and deformation bands specific to the materials studied.

At this Mara site, essential microorganisms are found on these materials, such as amino acids discovered associated with minerals loaded with nanoparticles, similar to comets from the fine molecular particles of the solar system. Samples M20P, M25P, M30P, and M35P are analyzed to determine the influence of the quantity of thermoplastics used.

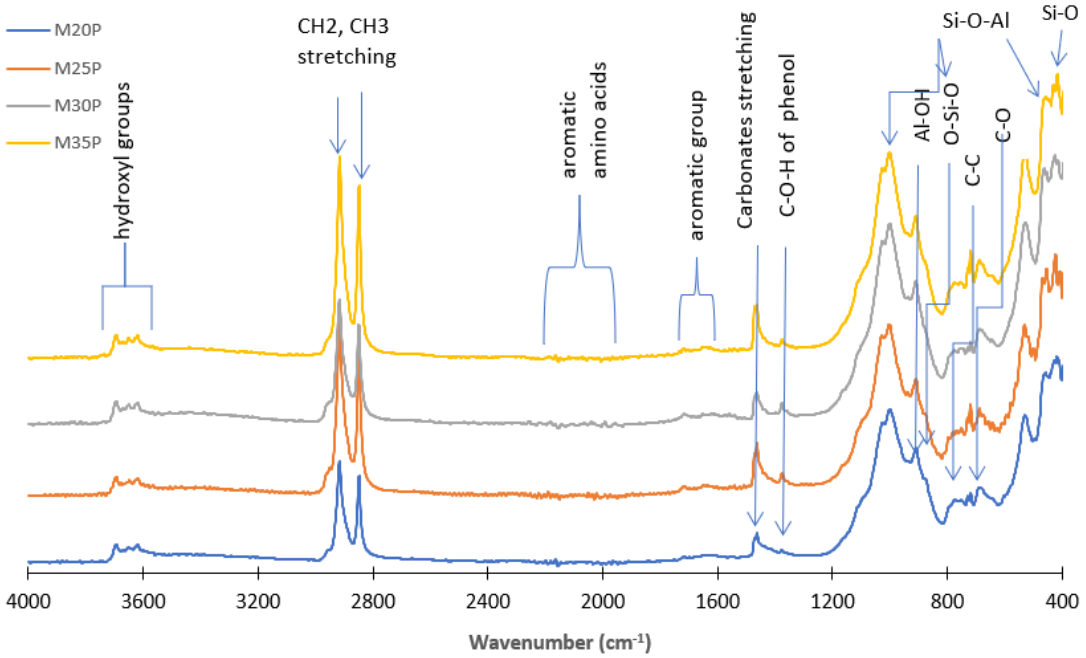

Figure 3. I R spectra of Mara samples.

Figure 3 presents the IR spectra of the four samples from the formulation M20P, M25P, M30P and M35P from the Mara site. Their structures are manifested through very intense peaks. The presence of thermoplastics consisting mainly of polyethylenes and polypropylenes did not influence the characteristic peaks of the said soil materials. Some bands find interpretations that are either on the mineral side or on the organic side. The absorption bands at frequencies between 415 and 530 cm^{-1} are assigned to the vibrations of the Si-O, Si-O-Al bonds. This indicates the presence of clay in the prepared mixtures. The out-of-plane C-OH bending of phenolic rings in a bonded state occurs as a typical band near 694 and 644 to 650 cm^{-1} [30]. This presence of clay materializes very specific bonds, such as the O-Si-O bonds in the silica tetrahedra around 910 cm^{-1} and 1000 cm^{-1}. Also, the peaks at 1000, 770 and 730 cm^{-1} belong to the C–C, C–O and C–H nuclei of the aromatic vibrations of the polymers [31]. On the other hand, specifically around 770 cm^{-1} it is quartz which asserts itself for the M20P formulation and at

775 cm^{-1} for M35P. In fact, these bands are those linked to the interaction between the clay sheets and the thermoplastic polymer. The presence of this recycled polymer will improve the hydrogen bond between the COOH groups and the oxides of the silicates [32] [33].

The fairly broad peaks at 1200 to 900 cm^{-1} represent traces of water incorporated into the nanopores of these samples. Their double sharp and broad aspects also materialize the aluminosilicate bonds in these samples. The density of these peaks varies depending on the percentage of polymers. The shoulders around 950 cm^{-1} are characteristic of stretching between mineral oxides and thermoplastic polymers in the presence [34].

According to one group, prodelphinins are characterized by a broad band at around 1350 cm^{-1}, a decrease in relative intensity in the region 1200 to 1030 cm^{-1} and an increase for the 1100 cm^{-1} band compared with the 1430 cm^{-1} band (46). Matching the degree of polymerization, all 4-(2',4',6'-trihydroxyphenyl) flavan–derivatives and the proanthocyanidin dimers are said to have in common a relatively intense band around 1150 cm^{-1} that is significantly weakened in the case of polymeric structures. With regard to the possible diasteroisomers, a diagnostic peak around 800 to 795 cm^{-1} is attributable to the trans configuration (catechin-based compounds), decreasing in intensity and showing a shoulder if a mixture the two isomers occurs. When this band shows the same intensity for the 770 or 730 cm^{-1} bands, the trans configuration is prevalent.

The characteristic peaks identified at 1467 cm^{-1} for M20P, 1462 cm^{-1} for M25P, and 1463 cm^{-1} for M30P and M35P all represent the stacked structures of the layers, responsible for the bonds at the clay-polymer interface. The same is true for the peaks at 2848 cm^{-1} and 2916 cm^{-1}. Each component undergoes a structural modification where the clay takes on an organo-modified configuration [35].

The bonds defined by these spectra, expressed by intense peaks, are those of the O-Si-O bonds in the silica tetrahedra.

The weak bands ranging from 1900 to 2300 cm^{-1} appear with the presence and increasing percentage of recycled thermoplastics; these peaks represent the amine groups. The weak band at 1633 cm^{-1} is specific to the vibration of OH groups of hydration water in the Mara soil. This same band is characteristic of oxides originating from smectite.

The stretching vibration bands ranging from 3694 cm^{-1} to 3649 cm^{-1} and 3620 cm^{-1}, characteristic of clay, are attributed to the interlayer hydroxyl groups of kaolinite. Furthermore, the presence of polymers indicates that these same peaks are those of groups belonging to the functional groups of amino acid derivatives and carboxylate groups of phenols. Their intensities and positions are generally sensitive to the intercalation of organic molecules. The characteristic band at 3620 cm^{-1} is specifically attributed to external hydroxyls with layers insensitive to intercalations. The presence of these significant vibrational bands suggests that this kaolinite extracted from this clayey soil in Mara exhibits a disordered structure [36] already elucidated by XRD.

Table 2. Wavenumber as a function of functional groups and vibration modes of Mara samples.

Wavenumber (cm^{-1})	*Functionals groups*
[900 - 1000]	Stretching of Al-O and Mg-O
1010 and 1110	O-Si-O Stretching
1467 for M20P 1462 for M25P 1463 for M30P and M35P	CH2 shear
2848 and 2916 for M20P, M25P and M35P 2849 and 2916 for M30P	CH2 Symmetric stretching
2929	CH2 Asymmetrical stretching
3636	Stretching of OH silicate

Table 2 lists all the bands observed in these spectra. Indeed, these formulations reveal a new geophysical state due to the change in vibrational energies and deformations at the atomic scale. This is why new peaks appear, thus generating shifts. These remarkable peaks are recorded in Table 2.

It should be noted that several bands correspond to both the mineral functions illustrated above by geochemistry and the amine functions from recycled thermoplastic polymers. We were unable to superimpose them on the different peaks in Figure 4. This is why the peak around 910 corresponds to both the deformation of the CH and bonds benzene ring vibrations in plane-ring deformation mode of phenolic ring [37]-[39] and to the Al-OH and Al-O-Si deformation vibration bands of kaolinite.

3.4. Thermal Analysis

Figures 4-7 present the TGA/TDA curves simultaneously, showing the mass losses of the four samples from the Mara site. Analysis of these curves reveals similar characteristics.

3.4.1. M35P Sample

Figure 4 represents the M35P sample. There is a glass transition phase at 125.27˚C accompanied by a mass loss of 0.28% on the TGA curve; this is due to the presence of thermoplastic polymers in the composite in question. This first phase corresponds to the hygroscopic departure of water within the illite sheets [40] with the first endothermic peak on the TDA curve at 125.27˚C. The second phase is marked by a long period of crystallization which goes from 125.27 to 482.73˚C. This long phase reflects the long duration of crosslinking of the amine bonds of the polymers combined with the rheology of the latter, to which must be added the oxides of the different constituents of the ores present. This phase is characterized by a mass loss of 16.69% for a temperature of 482.73˚C. Between 482.73˚C and 511.27˚C, a second endothermic peak (497.35˚C) is recorded, marking a new phase of recrystallization of the various constituents followed by mineralogical transformation. This phase is also attributable to the decomposition of organic

matter and hydroxides. Mineralogically, this temperature range corresponds to the hydroxylation of kaolinite and then its transformation into meta-kaolinite.

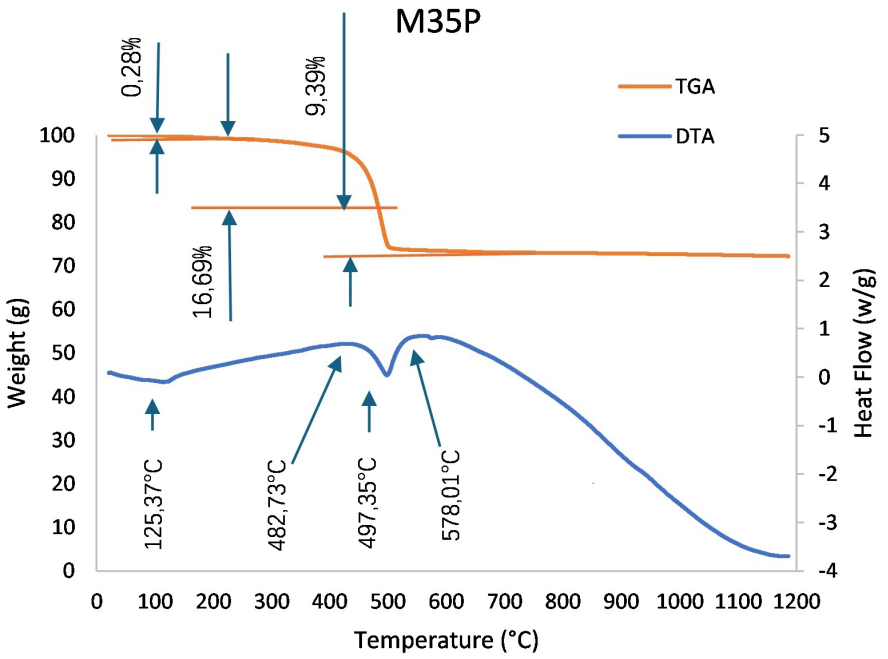

Figure 4. TGA /TDA analysis of M35P sample.

It is always at this temperature range that we observe the release of hydroxide formed during the crosslinking of bonds made up of oxide networks from the ores previously identified by geochemistry and XRD. These oxides are responsible for the presence of kaolinite, illite and quartz [41] [42]. It should also be noted on this second endothermic peak that this is the temperature at which the material loses most of its essential constituents, with an overall mass loss of 26.08%.

It should be noted that this very slow diffusion of heat during the temperature rise, still characterized by a slight loss of mass of its constituents, can be a major asset against the kinetics of water propagation in the material. This is one of the objectives of this work because flooding has an impact on the constructions of these vulnerable areas. Between 511.27˚C and 612.26˚C, an attempt to regain the material's capacity is visible through recrystallization up to a temperature of 578.01˚C. Beyond this temperature, precisely at 584.11˚C, the total melting of the material begins, marked by a continual drop in the DTA curve. This phase is remarkable with the TGA curve tending asymptotically and horizontally up to 1200˚C.

3.4.2. M30P Sample

The M30P sample in **Figure 5** shows some similarities in shape with the previous one. The TGA curve has the same shape and the DTA has a small difference. A slight concavity instead of an endothermic peak is noticeable around 96.37˚C. It corresponds to a slight glass transition phase due to the small amount of polymer

in this sample taken. It corresponds to a mass loss of 0.21% recorded on the TGA curve. It is also the hygroscopic departure of the water molecules incorporated in the illite sheets present in the ores found there. Beyond this first temperature range, there is a very rapid increase in temperature up to 442.08˚C. This temperature threshold corresponds to the beginning of the rapid mass degradation phase of this sample. This mass loss reaches its peak at 510.15˚C. At this same temperature, the true endothermic peak is recorded on the DTA curve. Beyond this temperature, the polymer interjected into the material tries to recrystallize, but unfortunately begins to melt at 571.01˚C. At this temperature, the material loses its essential constituents and turns into ash. During this time, the TGA curve has lost a total of 19.60˚C of its constituents and becomes almost horizontal. This means that temperature no longer has any effect on the material.

Mineralogically, the same interpretation as the previous one emerges, namely the hydroxylation of kaolinite and its transformation into meta-kaolinite around 510.15˚C. It is also around this temperature that we observe the release of hydroxide formed during the crosslinking of the bonds made up of oxide networks from kaolinite, illite and quartz.

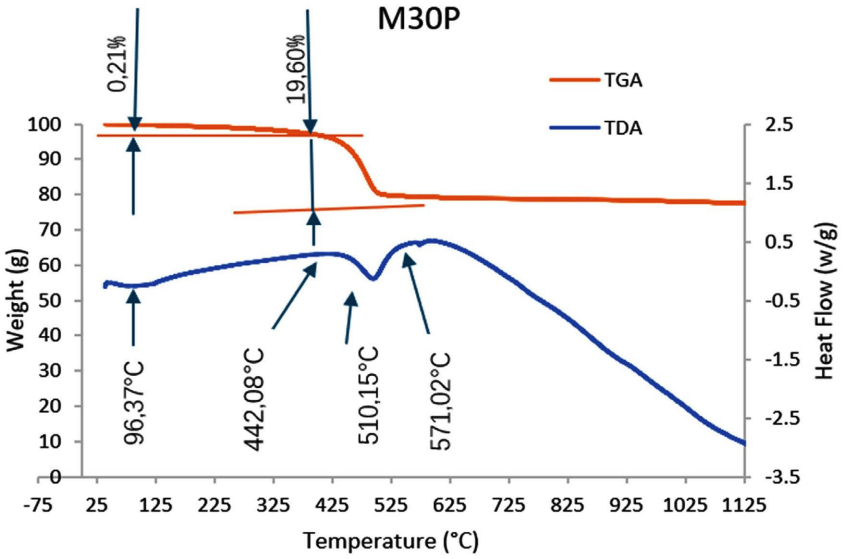

Figure 5. TGA /TDA analysis of M30P sample.

3.4.3. M25P Sample

The particularity of this sample, unlike the two previous ones, is that it presents an almost linear ascending curve, from room temperature to 431.23˚C on the DTA curve. At this same temperature, a mass loss of 04.61% is recorded on the TGA curve. The absence of a transition phase over this long temperature range can be explained by the small quantity of polymer on the one hand, and on the other hand, one can question the quality of the homogenization of the mixture which could have defects. Indeed, in most materials obtained by mixing several components, there are always places called "grey zones" where homogenization is

not well ensured. They are at the origin of the first starting points of structural defects in composites. The clearly perceptible endothermic peak is at 494.82˚C. in fact, from 431.61˚C to 494.82˚C, the entire mass loss of 19.17% is recorded on the TGA curve. This explains the low presence of the polymer and the evaporation of its constituents. We note with the TGA curve that beyond 494.82˚C, the material no longer loses mass. This also explains the total and sudden departure of the essential constituents of the ores. The total melting is recorded. The TGA curve becomes horizontal and that of the DTA descends continuously at a low slope from 592.87˚C until the end of the test at 1200˚C.

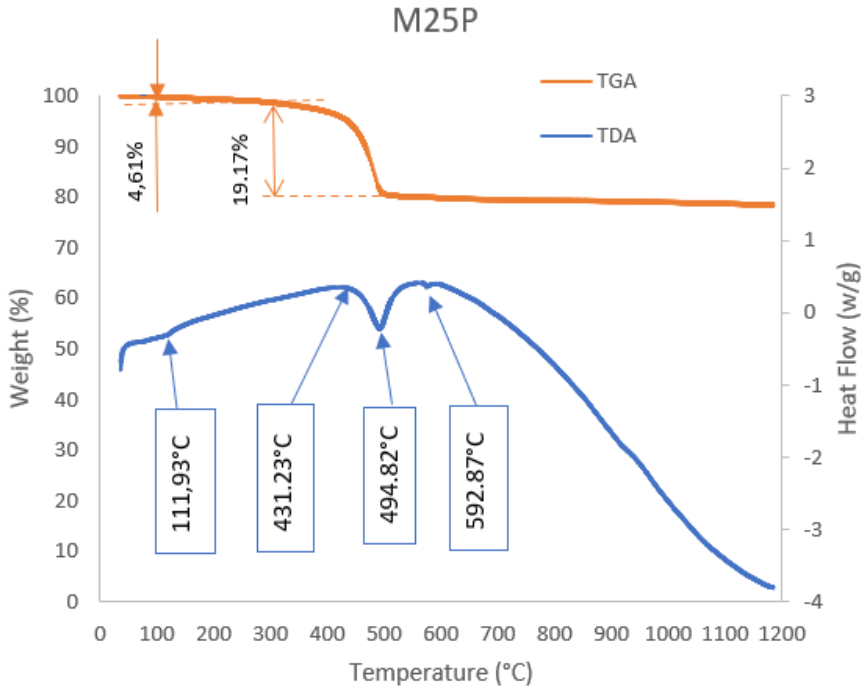

Figure 6. TGA /TDA analysis of M25P sample.

3.4.4. M20P Sample

Sample M20P would like to be assimilated to M35P according to the DTA curve. However, the low amount of polymer (20%) within the material prevailed. This is why an overall mass loss of 14.54% is recorded on its TGA curve. This mass loss is obtained at a temperature of 491.13˚C. It began at 114.13˚C with a slight value of around 0.93%; then it dropped sharply to 458.97˚C. This is manifested on both curves by a maximum on the DTA curve, marking the end of the long polymer crystallization phase. For the ores present, this temperature corresponds to the transformation phase of kaolinite into metakaolinite. It also marks the release of hydroxides formed during the crosslinking of bonds made up of several oxide networks formed by kaolinite, illite and quartz. At 580.64˚C, the material has completely declined. More mass loss is recorded and the TGA curve becomes horizontal; the DTA curve decreases continuously up to 1200˚C.

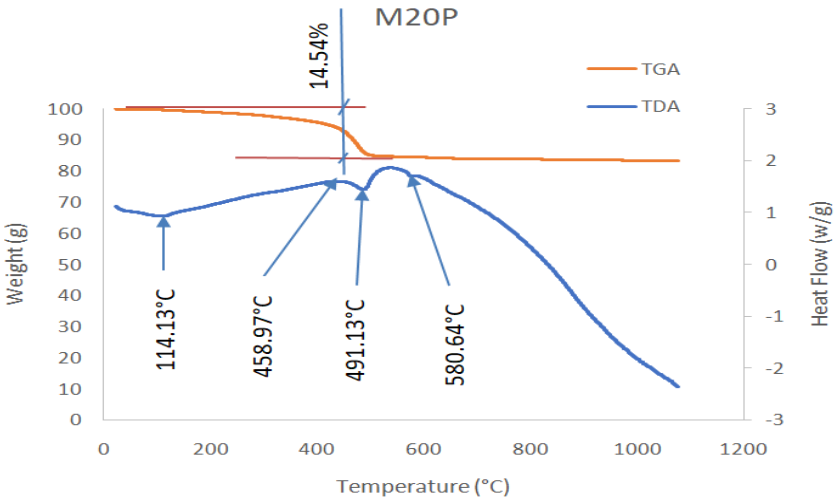

Figure 7. TGA /TDA analysis of M20P sample.

Overall, the transformations of the ores present under the influence of temperature allowed the different constituents to crystallize and acquire the expected physical and mechanical properties. Indeed, for the four samples M35P, M30P, M25P and M20P, the temperature range varying from 120˚C to 500˚C is indicated for the structural transformation within the material. This is the temperature range where all these samples are in the crystallization phase. The incorporated polymers resume their function by activating the functional groups under the effect of temperature, awaiting the realization of future chemical bonds. The oxides, for their part, undergo transformations to give rise to secondary ores. The dissolution of silica and alumina, for example, finds an activation factor through the rheological character of the thermoplastic polymer. The latter ensures a dual function, namely its ability to move in fine cavities within the material, thus solving the crucial problem of porosity which is at the origin of the early deterioration of earth bricks. The second factor lies in its ability to establish strong bonds with the oxides of mineral origin during their transformation phase. Indeed, during cooling, the polymer consolidates by forming rigid contacts with the crystallized particles of oxides from silica, illite, feldspar, kaolinite and other calcites present. The material thus constituted will have the chance to overcome the effects of water absorption linked to porosities which would cause rupture phenomena within the bricks designed without these significant contributions of recycled polypropylenes.

The resins quantity in the reinforced materials made of powder particles is generally around 20% [43]. Below this value, the consolidation of the composite is no longer ensured due to the very insufficient amount of resin. The dissolution of oxides could also be conditioned by the flow-through capacity of the matrix resin. Therefore, one would be tempted to increase as much as possible the quantity of thermoplastics to ensure an activation solution for silica and alumina in particular, which could also play the role of pore filling. This could also improve the microstructure of the geopolymer formed and increase its physical and mechanical performances [44] [45].

3.5. Physical and Mechanical Properties

These physical and mechanical results are intended to verify that the predictions made from the microstructural analyses of XRD, ATR FTIR, and TGA/DTA are as expected.

3.5.1. Water Absorption

The assessment conducted for this work in terms of the dosage of the recovered thermoplastic polymer remains within the predictive aspect of the behavior to be discovered from the microstructural analyses. Unlike the destructive power that water often has on geopolymers, it was predicted that the infiltration of the thermoplastic matrix such as polyethylene and polypropylene into the micropores could prevent the breakdown of the mechanical bonds established during sample compaction.

Figure 8 and Figure 9 show the evolution of the water absorption rate as a function of the immersion time, measured in days. It appears that all samples absorb water rapidly on the first day. This is explained by the filling of the micropores observed across the entire exterior surface of each sample. A slow progression of water is subsequently observed, with the slopes of these curves becoming increasingly shallow with increasing days. These curves end asymptotically, indicating their saturation.

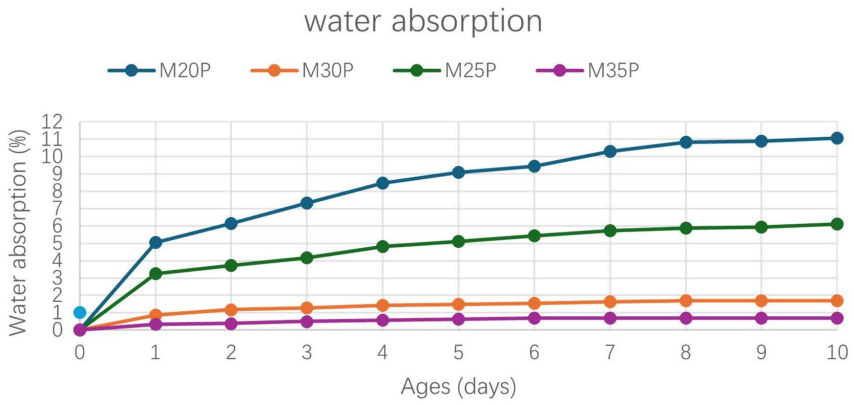

Figure 8. Water absorption as a function of polymer quantity at Mara.

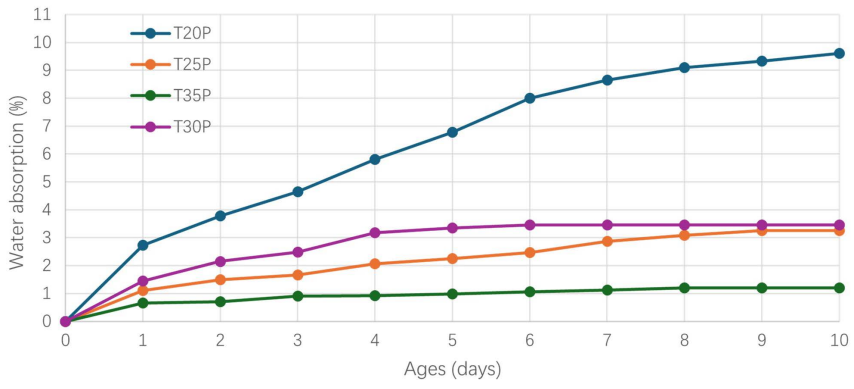

Figure 9. Water absorption as a function of the quantity of polymers in Toukra.

3.5.2. Uni Axial Compression

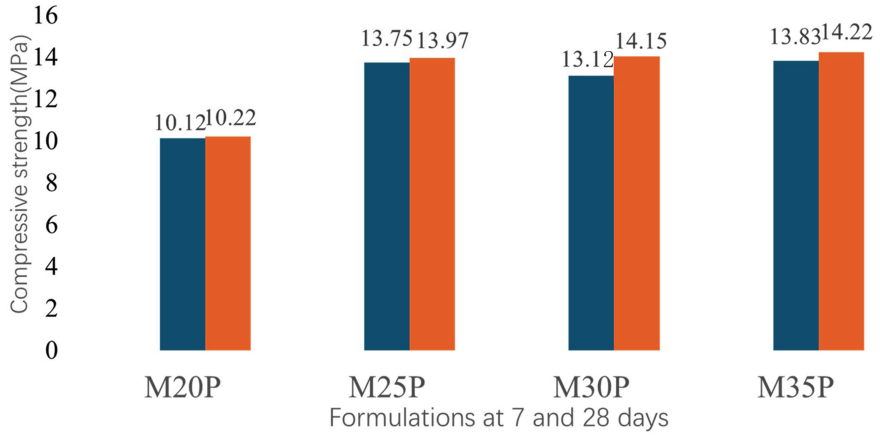

Figure 10. Compressive strength (Mara).

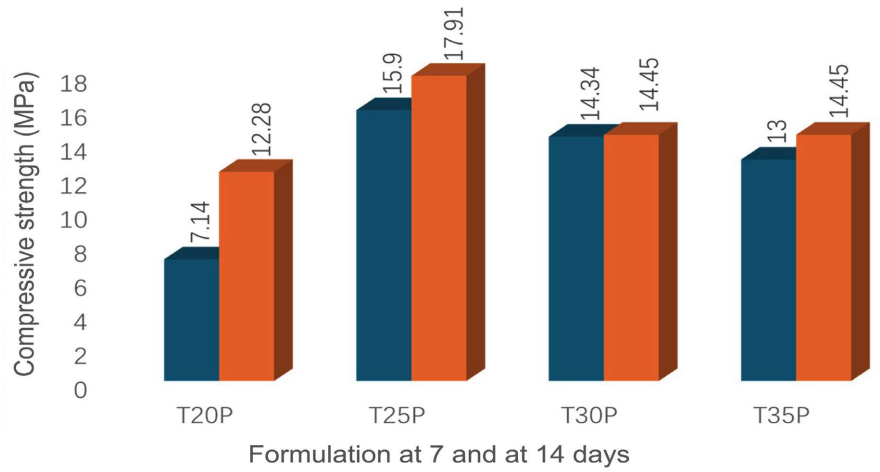

Figure 11. Compressive strength (Toukra).

Figure 10 and Figure 11 display histograms showing the ultimate strength values for each sample. At the Mara site, the highest value observed was for the M35P formulation, which corresponds to the highest dosage of thermoplastics used. The lowest value was for the M20P formulation. It should be noted that all of these formulations performed well with the presence of this polymer. An average of 12.85 MPa was recorded for these four samples.

For the samples from the Toukra site, an average compressive strength of 15.52 MPa was recorded. The highest value, 15.65 MPa, was observed for the M25P formulation, and the lowest, 12.28 MPa, was observed for the M20P samples. These better results are explained by the fact that the Toukra site contains a large quantity of quartz [11] (compared to the Mara site), an essential constituent of silica. Under thermal effects, the rheological action of thermoplastics finds good compatibility with the crystallized silica particles to establish the recommended bonds.

Recycled polypropylene and polyethylene matrix earth brick composites have

higher compressive mechanical properties than those associated with filaments [46]-[48]. This increase in compressive strength indicates that the effect of reinforcing the clay load by thermoplastics in melting at temperature is of considerable contribution. Indeed, the confinement of this matrix inside the clay sheets allowed the stabilization of the chain segments produced during compaction, which made it possible to improve the tensile mechanical resistance [49]-[51].

4. Conclusion

This work suggests that the improved mechanical properties of earth bricks combined with recycled polypropylene and polyethylene thermoplastics can be attributed to compatibility between the clay layers and the molecular chains derived from these polymers. These results were predicted by microstructural interpretations of these samples. Indeed, investigations conducted on the materials from both sites began with geochemistry, which revealed the presence of silica oxides (SiO_2) (57.28% - 65.81%), aluminum oxides (Al_2O_3) (12.29% - 14.40%), and iron oxides (Fe_2O_3) (6.16% - 9.23%) as major elements. Alkali and alkaline earths such as potassium K_2O (3.64% - 4.10%), titanium TiO_2 (1.09% - 1.40%), sodium Na_2O (1.08% - 1.26%), calcium CaO (1.05% - 2.61%), magnesium MgO (0.73% appear in small quantities. These oxides come from quartz, kaolinite, feldspar, illite and many others confirmed by DRX, ATR FTIR and TGA/DTA. The vibrational movements observed with the presence of polypropylenes and polyethylenes favored physicochemical interactions with mineral oxides. The rheological character of this polymer matrix made it possible to plug the micropores in the clay sheets by acting in a compatible manner with the oxides present. This allowed us to predict good water absorption behavior and good mechanical performance. Some formulations provided less than 2% water absorption in 10 days of immersion. The compressive strength varies from 10.22 to 14.22 MPa at the Toukra site and from 12. 17.35 MPa at Mara. In the future, we can explore a simulation of these different formulations and model them to expect better results.

Conflicts of Interest

The authors declare no conflicts of interest regarding the publication of this paper.

References

[1] Ndong, A.T., Ndiaye, O., Sagna, M.B., Diallo, A., Galop, D. and Guisse, A. (2015) Caractérisation de la végétation ligneuse sahélienne du Sénégal: Cas du Ferlo. *International Journal of Biological and Chemical Sciences*, **9**, 2582-2594. https://doi.org/10.4314/ijbcs.v9i6.6

[2] Kissou, R., Gnankambary, Z., Nacro, H.B. and Sedogo, M.P. (2018) Classification locale et utilisation des sols en zone sahélienne au Burkina Faso. *International Journal of Biological and Chemical Sciences*, **12**, 610-617. https://doi.org/10.4314/ijbcs.v12i1.46

[3] He, I.L., Atheba, G.P., Allou, N.B., Drogui, P., Khakani, M.A.E. and Gbassi, G.K. (2023) Physic, Chemical and Mineralogical Characterizations of Clays Used in the

Making of Traditional Ceramics in the City of Katiola, Côte d'Ivoire. *Journal of Minerals and Materials Characterization and Engineering*, **11**, 81-91. https://doi.org/10.4236/jmmce.2023.114008

[4] Kagonbé, B.P., Tsozué, D., Nzeukou, A.N. and Ngos, S. (2021) Mineralogical, Physico-Chemical and Ceramic Properties of Clay Materials from Sekandé and Gashiga (North, Cameroon) and Their Suitability in Earthenware Production. *Heliyon*, **7**, e07608. https://doi.org/10.1016/j.heliyon.2021.e07608

[5] Tsozué, D., Nzeugang, A.N., Mache, J.R., Loweh, S. and Fagel, N. (2017) Mineralogical, Physico-Chemical and Technological Characterization of Clays from Maroua (Far-North, Cameroon) for Use in Ceramic Bricks Production. *Journal of Building Engineering*, **11**, 17-24. https://doi.org/10.1016/j.jobe.2017.03.008

[6] Nshimiyimana, P., Fagel, N., Messan, A., Wetshondo, D.O. and Courard, L. (2020) Physico-Chemical and Mineralogical Characterization of Clay Materials Suitable for Production of Stabilized Compressed Earth Blocks. *Construction and Building Materials*, **241**, Article 118097. https://doi.org/10.1016/j.conbuildmat.2020.118097

[7] Bentahar, Y., Draoui, K., Hurel, C., Ajouyed, O., Khairoun, S. and Marmier, N. (2019) Physico-Chemical Characterization and Valorization of Swelling and Non-Swelling Moroccan Clays in Basic Dye Removal from Aqueous Solutions. *Journal of African Earth Sciences*, **154**, 80-88. https://doi.org/10.1016/j.jafrearsci.2019.03.017

[8] Kagonbé, B.P., Nafissa, B., Djeutchou, C., Hamdja, A.N., Djoda, P., Loabé, A.P., *et al.* (2024) Gravel and River Sand Mining Activities in Maroua (Far-North Region, Cameroon): Environmental and Socioeconomic Aspects. *Archives of Agriculture and Environmental Science*, **9**, 126-133. https://doi.org/10.26832/24566632.2024.0901018

[9] Abreu, A.S., Oliveira, M. and Machado, A.V. (2015) Effect of Clay Mineral Addition on Properties of Bio-Based Polymer Blends. *Applied Clay Science*, **104**, 277-285. https://doi.org/10.1016/j.clay.2014.12.006

[10] Madjihingam, N., Pagore, D., Mache, J.R., Warabi, B., Kagonbe, B.P. and Kouotou, P.M. (2024) Clay Materials for Ceramics Application from N'Djamena in the Chad Republic: Mineralogical, Physicochemical and Microstructural Characterization. *Journal of Materials Science and Chemical Engineering*, **12**, 31-48. https://doi.org/10.4236/msce.2024.122003

[11] Bebbata, W., Djoda, F.P., Ndjolba, M., Kagonbé, B.P. and Danwé, R. (2024) Geochemistry and Microstructure of Construction Materials from the Eastern Districts of N'Djamena Chad with a View to Their Stabilization in the Building and Pottery. *Materials Sciences and Applications*, **15**, 431-449. https://doi.org/10.4236/msa.2024.1510029

[12] Muñiz-Villarreal, M.S., Manzano-Ramírez, A., Sampieri-Bulbarela, S., Gasca-Tirado, J.R., Reyes-Araiza, J.L., Rubio-Ávalos, J.C., *et al.* (2011) The Effect of Temperature on the Geopolymerization Process of a Metakaolin-Based Geopolymer. *Materials Letters*, **65**, 995-998. https://doi.org/10.1016/j.matlet.2010.12.049

[13] Zribi, M. and Baklouti, S. (2021) Investigation of Phosphate Based Geopolymers Formation Mechanism. *Journal of Non-Crystalline Solids*, **562**, Article 120777. https://doi.org/10.1016/j.jnoncrysol.2021.120777

[14] Pandey, S. and Mishra, S.B. (2011) Sol-Gel Derived Organic-Inorganic Hybrid Materials: Synthesis, Characterizations and Applications. *Journal of Sol-Gel Science and Technology*, **59**, 73-94. https://doi.org/10.1007/s10971-011-2465-0

[15] Malucelli, G. (2016) Hybrid Organic/Inorganic Coatings through Dual-Cure Processes: State of the Art and Perspectives. *Coatings*, **6**, Article 10. https://doi.org/10.3390/coatings6010010

[16] Moussout, H., Ahlafi, H., Aazza, M., Chfaira, R. and Mounir, C. (2020) Interfacial Electrochemical Properties of Natural Moroccan Ghassoul (Stevensite) Clay in Aqueous Suspension. *Heliyon*, **6**, e03634. https://doi.org/10.1016/j.heliyon.2020.e03634

[17] Linker, R., Kenny, A., Shaviv, A., Singher, L. and Shmulevich, I. (2004) Fourier Transform Infrared—Attenuated Total Reflection Nitrate Determination of Soil Pastes Using Principal Component Regression, Partial Least Squares, and Cross-Correlation. *Applied Spectroscopy*, **58**, 516-520. https://doi.org/10.1366/000370204774103327

[18] Cases, J., Liétard, O., Yvon, J. and Delon, J. (1982) Étude des propriétés cristallochimiques, morphologiques, superficielles de kaolinites désordonnées. *Bulletin de Minéralogie*, **105**, 439-455. https://doi.org/10.3406/bulmi.1982.7566

[19] Morris, J.H., Perkins, P.G., Rose, A.E.A. and Smith, W.E. (1977) The Chemistry and Binding Properties of Aluminium Phosphates. *Chemical Society Reviews*, **6**, 173-194. https://doi.org/10.1039/cs9770600173

[20] Barbhuiya, S. and Pang, E. (2022) Strength and Microstructure of Geopolymer Based on Fly Ash and Metakaolin. *Materials*, **15**, Article 3732. https://doi.org/10.3390/ma15103732

[21] Chen, L., Wang, Z., Wang, Y. and Feng, J. (2016) Preparation and Properties of Alkali Activated Metakaolin-Based Geopolymer. *Materials*, **9**, Article 767. https://doi.org/10.3390/ma9090767

[22] Duxson, P., Provis, J.L., Lukey, G.C., Mallicoat, S.W., Kriven, W.M. and van Deventer, J.S.J. (2005) Understanding the Relationship between Geopolymer Composition, Microstructure and Mechanical Properties. *Colloids and Surfaces A*: *Physicochemical and Engineering Aspects*, **269**, 47-58. Https://Doi.Org/10.1016/J.Colsurfa.2005.06.060

[23] Wang, W., Fan, C., Wang, B., Zhang, X. and Liu, Z. (2023) Workability, Rheology, and Geopolymerization of Fly Ash Geopolymer: Role of Alkali Content, Modulus, and Water-Binder Ratio. *Construction and Building Materials*, **367**, Article 130357. https://doi.org/10.1016/j.conbuildmat.2023.130357

[24] Wang, Q., Odlyha, M. and Cohen, N.S. (2000) Thermal Analyses of Selected Soil Samples from the Tombs at the Tianma-Qucun Site, Shanxi, China. *Thermochimica Acta*, **365**, 189-195. https://doi.org/10.1016/s0040-6031(00)00723-1

[25] Cook, H.E., Johnson, P.D., Matti, J.C. and Zemmels, I. (1975) Methods of Sample Preparation and X-Ray Diffraction Data Analysis. X-Ray Mineralogy Laboratory, Deep Sea Drilling Project, University of California, Riverside. U.S. Government Printing Office, 999-1007. https://doi.org/10.2973/dsdp.proc.28.app4.1975

[26] Fagel, N., Boski, T., Likhoshway, L. and Oberhaensli, H. (2003) Late Quaternary Clay Mineral Record in Central Lake Baikal (Academician Ridge, Siberia). *Palaeogeography*, *Palaeoclimatology*, *Palaeoecology*, **193**, 159-179. https://doi.org/10.1016/s0031-0182(02)00633-8

[27] Kagonbé, B.P., Tsozué, D., Nzeukou, A.N. and Ngos III, S. (2021) Mineralogical, Geochemical and Physico-Chemical Characterization of Clay Raw Materials from Three Clay Deposits in Northern Cameroon. *Journal of Geoscience and Environment Protection*, **9**, 86-99. https://doi.org/10.4236/gep.2021.96005

[28] Tsozué, D., Nzeukou, A.N., Kagonbé, B.P., Madi, A.B., Mache, J.R., Bitom, D.L., *et al.* (2022) Genesis and Assessment of Clay Materials Suitability for Earthenware Production in Northern Cameroon. *Arabian Journal of Geosciences*, **15**, Article No. 1376. https://doi.org/10.1007/s12517-022-10603-7

[29] Nzeukou Nzeugang, A., Tsozué, D., Kagonbé Pagna, B., Balo Madi, A., Fankam Deumeni, A., Ngos, S., *et al.* (2021) Clayey Soils from Boulgou (North Cameroon):

Geotechnical, Mineralogical, Chemical Characteristics and Properties of Their Fired Products. *SN Applied Sciences*, **3**, Article No. 551. https://doi.org/10.1007/s42452-021-04541-4

[30] Pardeshi, S., Dhodapkar, R. and Kumar, A. (2013) Quantum Chemical Density Functional Theory Studies on the Molecular Structure and Vibrational Spectra of Gallic Acid Imprinted Polymers. *Spectrochimica Acta Part A*: *Molecular and Biomolecular Spectroscopy*, **116**, 562-573. https://doi.org/10.1016/j.saa.2013.07.067

[31] Murugananthan, M., Bhaskar Raju, G. and Prabhakar, S. (2005) Removal of Tannins and Polyhydroxy Phenols by Electro-Chemical Techniques. *Journal of Chemical Technology & Biotechnology*, **80**, 1188-1197. https://doi.org/10.1002/jctb.1314

[32] Zhang, X., Cai, Y., Jiang, D., Zhang, Y., Pan, Y. and Bai, L. (2017) An Experimental Study on Transforming Montmorillonite to Glauconite: Implications for the Process of Glauconitization. *Clays and Clay Minerals*, **65**, 431-448. https://doi.org/10.1346/ccmn.2017.064081

[33] Zhang, Y., Lee, J., Jang, H. and Nah, C. (2004) Preparing PP/Clay Nanocomposites Using a Swelling Agent. *Composites Part B*: *Engineering*, **35**, 133-138. https://doi.org/10.1016/s1359-8368(03)00068-4

[34] Dabbebi, R., de Aguiar, J.L.B., Samet, B. and Baklouti, S. (2019) Mineralogical and Chemical Investigation of Tunisian Phosphate Washing Waste during Calcination. *Journal of Thermal Analysis and Calorimetry*, **137**, 1827-1840. https://doi.org/10.1007/s10973-019-08057-3

[35] Mansoori, Y., Akhtarparast, A., Reza Zamanloo, M., Imanzadeh, G. and Masooleh, T.M. (2011) Polymer-Montmorillonite Nanocomposites: Chemical Grafting of Polyvinyl Acetate onto Cloisite 20A. *Polymer Composites*, **32**, 1225-1234. https://doi.org/10.1002/pc.21142

[36] Frost, R.L. and Vassallo, A.M. (1996) The Dehydroxylation of the Kaolinite Clay Minerals Using Infrared Emission Spectroscopy. *Clays and Clay Minerals*, **44**, 635-651. https://doi.org/10.1346/ccmn.1996.0440506

[37] Hu, F., Zhang, Y., Zhang, H., Li, L. and Tian, A. (2010) Density Functional Theory Study on Hydrogen Bonding Interaction of Catechin-$(H_2O)_n$. *Chinese Journal of Chemistry*, **28**, 741-747. https://doi.org/10.1002/cjoc.201090140

[38] Komal Kumar, J. and Devi Prasad, A.G. (2011) Identification and Comparison of Biomolecules in Medicinal Plants of Tephrosia Tinctoria and Atylosia Albicans by Using FTIR. *Romanian Journal of Biophysics*, **21**, 63-71.

[39] Balan, E., Lazzeri, M., Morin, G. and Mauri, F. (2006) First-Principles Study of the OH-Stretching Modes of Gibbsite. *American Mineralogist*, **91**, 115-119. https://doi.org/10.2138/am.2006.1922

[40] Mielenz, R.C., Schieltz, N.C. and King, M.E. (1953) Thermogravimetric Analysis of Clay and Clay-Like Minerals. *Clays and Clay Minerals* (*National Conference on Clays and Clay Minerals*), **2**, 285-314. https://doi.org/10.1346/ccmn.1953.0020124

[41] Michot, A. (2008) Caractéristiques thermophysiques de matériaux à base d'argile: Évolution avec des traitements thermiques jusqu'à 1400˚C. Master's Thesis, Université de Limoges.

[42] Letellier, M.C. (1986) Récupération et dosage des phases argileuses d'un sable de gisement. Ph.D. Thesis, University of Toulouse.

[43] Pagoré, F.D., Saïdjo, Makomra, V., Kada, A.D., Ntenga, R. and Ohandja, L.-M.A. (2025) Microstructural, Physico-Mechanical and Thermal Characterization of Materials Based on Epoxy Resin Reinforced of Palm Kernel Shell Powder Tenera Type for a View to a Structural Application. *World Journal of Advanced Research and Reviews*,

25, 1471-1485. https://doi.org/10.30574/wjarr.2025.25.3.0853

[44] Phoo-Ngernkham, T., Chindaprasirt, P., Sata, V., Hanjitsuwan, S. and Hatanaka, S. (2014) The Effect of Adding Nano-SiO_2 and Nano-Al_2O_3 on Properties of High Calcium Fly Ash Geopolymer Cured at Ambient Temperature. *Materials & Design*, **55**, 58-65. https://doi.org/10.1016/j.matdes.2013.09.049

[45] Ibrahim, M., Johari, M.A.M., Maslehuddin, M. and Rahman, M.K. (2018) Influence of Nano-SiO_2 on the Strength and Microstructure of Natural Pozzolan Based Alkali Activated Concrete. *Construction and Building Materials*, **173**, 573-585. https://doi.org/10.1016/j.conbuildmat.2018.04.051

[46] Zdiri, K. (2019) Synthèse de composites à base de PP recyclé-Argile pour des applications textiles. Université de Haute Alsace-Mulhouse, École nationale d'Ingénieurs de Monastir.

[47] Masuka, S., Gwenzi, W. and Rukuni, T. (2018) Development, Engineering Properties and Potential Applications of Unfired Earth Bricks Reinforced by Coal Fly Ash, Lime and Wood Aggregates. *Journal of Building Engineering*, **18**, 312-320. https://doi.org/10.1016/j.jobe.2018.03.010

[48] Izemmouren, O., Guettala, A. and Guettala, S. (2015) Mechanical Properties and Durability of Lime and Natural Pozzolana Stabilized Steam-Cured Compressed Earth Block Bricks. *Geotechnical and Geological Engineering*, **33**, 1321-1333. https://doi.org/10.1007/s10706-015-9904-6

[49] Hasegawa, N. and Usuki, A. (2004) Silicate Layer Exfoliation in Polyolefin/Clay Nanocomposites Based on Maleic Anhydride Modified Polyolefins and Organophilic Clay. *Journal of Applied Polymer Science*, **93**, 464-470. https://doi.org/10.1002/app.20459

[50] Biswal, M., Mohanty, S. and Nayak, S.K. (2011) Effect of Mercerized Banana Fiber on the Mechanical and Morphological Characteristics of Organically Modified Fiber-Reinforced Polypropylene Nanocomposites. *Polymer-Plastics Technology and Engineering*, **50**, 1458-1469. https://doi.org/10.1080/03602559.2011.593079

[51] Rabiei, N., Kish, M.H., Amirshahi, S.H. and Radjabian, M. (2012) The Kinetic and Thermodynamic Parameters of Dyeing of Polypropylene/Clay Composite Fibers Using Disperse Dye. *Dyes and Pigments*, **94**, 386-392. https://doi.org/10.1016/j.dyepig.2012.02.010